

A MICROWAVE-BASED SENSOR FOR NON-CONTACT MEASUREMENT OF WATER AND CRUDE OIL MIXTURE VOLUME RATIOS

Abdulilah Mohammad Mayet¹⁾, Salman Arafath Mohammed¹⁾, Robert Hanus²⁾,
Shamimul Qamar³⁾, Hassen Loukil¹⁾, Neeraj K. Shukla¹⁾

1) Electrical Engineering Department, King Khalid University, Abha 61411, Saudi Arabia

2) Rzeszów University of Technology, Faculty of Electrical and Computer Engineering, Powstańców Warszawy 12, 35-959 Rzeszów, Poland
(✉ rohan@prz.edu.pl)

3) Department of Computer Science and Engineering, Applied College, Dhahran Al Janoub Campus, King Khalid University, Abha 61411, Saudi Arabia

Abstract

This work presents the design, fabrication, and characterization of a novel microwave-based sensor utilizing multiple U-shaped resonators for non-contact measurement of volume percentages in water-crude oil mixtures. The sensor, fabricated on an RT/Duroid 4003 substrate ($\epsilon_r = 3.55$, thickness 0.787 mm), operates in the 2–2.3 GHz frequency range with a maximum insertion loss of 0.97 dB. Design optimization and electromagnetic simulations were performed using ADS software, followed by experimental validation with 10 ml samples of varying water content (0–100%) placed in a 3D-printed PLA container. Significant shifts in center frequency and response prominence were observed, enabling clear differentiation of mixture compositions. The sensor achieved a high sensitivity of 4.12 MHz/ ϵ_r , surpassing many prior designs, while the non-contact configuration enhances practicality by minimizing contamination risks and interference. Although highly sensitive and compact, potential limitations include dependence on crude oil composition variability, temperature effects, and the fixed sample volume used in testing. These results demonstrate the sensor's reliability for real-time fluid analysis, with promising applications in petroleum, chemical, and environmental monitoring industries.

Keywords: non-contact measurement, volume percentage, crude oil and water solution, microwave sensor, high sensitivity.

1. Introduction

In recent years, the application of microstrip sensors for analyzing water and petroleum-based substances has gained significant attention due to their potential for precise, compact, and non-invasive measurement techniques. Han *et al.* [1] proposed a microfluidic microwave sensor using an annular microstrip patch for evaluating the quality of lubricating oils. The strength of this work lies in the integration of a microfluidic structure, enhancing its sensitivity and enabling real-time monitoring. However, its limited operational frequency range restricts its application to specific oil types. Sattari and Hayati [2] introduced a non-contact microstrip sensor enhanced with artificial neural networks to estimate oil-water ratios regardless of sample volume. This method demonstrated high accuracy and flexibility, yet the reliance on trained models could limit its generalizability to unseen fluid types or conditions. In a follow-up work, the same authors [3] developed a similar antenna-based sensor incorporating the *Group Method of Data Handling* (GMDH) neural network for improved data modeling. The design was notable for combining machine learning with microstrip design, though fabrication complexity and model training overhead were limitations. Xue *et al.* [4] presented a flexible microstrip sensor capable of simultaneously measuring acid and water contamination in oils. The major advantage was its flexibility and dual-parameter sensing. Nevertheless, the system's fabrication

required complex materials, increasing cost and reducing ease of deployment. Abdulsattar *et al.* [5] designed an optical-microwave hybrid sensor for detecting water content in oil derivatives. Their work was innovative in combining different sensing modalities for higher accuracy, but integration and calibration challenges limited its practical scalability. Palandoken and Gocen [6] reviewed advances in microwave sensors for liquid dielectric characterization. Although it was not experimental research, the paper provided a comprehensive survey and performance comparison of modern designs, offering valuable insights for future development. Its main shortcoming was the lack of direct implementation results. Jin *et al.* [7] focused on measuring water holdup in oil-in-water emulsions using microwave resonance sensors in wellbores. Their system addressed in-situ monitoring under harsh conditions, showing robustness. However, it lacked compactness, which is critical in sensor miniaturization efforts. Wang *et al.* [8] utilized microstrip antennas to monitor oil–gas–water slug flow composition. The method achieved good temporal resolution and accuracy in multiphase flows. Still, its design was more suitable for large industrial systems than portable applications. Zhu *et al.* [9] designed a flexible substrate-integrated microstrip sensor for detecting moisture in lubricating oil. It offered advantages in flexibility and low-cost fabrication. The limitation was its relatively narrow application domain, focusing mainly on moisture rather than comprehensive fluid analysis.

To measure water-cut in crude oil emulsions in real-time without touching the sample, scientists created a chipless planar microwave sensor that uses a passive split-ring resonator. This sensor shows frequency shifts of about 70 MHz throughout the whole water-cut range and allows for high-resolution monitoring with little sample volume needed [10]. Researchers have developed a sensor that uses a multilayer perceptron neural network and a substrate-integrated waveguide resonator to detect and quantify water contamination in fuel oil without damaging the oil. This sensor has sensitivity levels of 0.12 dB/% and 0.88 MHz/% across concentrations ranging from 0% to 100% [11]. To improve sensitivity and noise immunity, Ebrahimi *et al.* [12] constructed a differential microstrip using split-ring resonators. Fabrication issues arise from the need for very symmetrical structures, which is its main restriction. By increasing sensitivity via intermodulation distortion, Abdolrazzaghi and Daneshmand [13] were able to detect minute changes in permittivity with remarkable accuracy. The complexity of the system and its dependence on oscillator stability are increased as a result. Using enhanced spectral data from transmission parameters, a convolutional neural network has been combined with a dual-passband microwave microstrip sensor to detect non-destructive milk spoiling in real-time. The training accuracy was 95.5% [14]. Engineers have designed a microstrip-coupled split-ring resonator sensor to detect impurities in lubricating oil. This sensor can identify stainless-steel particles (with a limit of 70 μm) and air bubbles (with a limit of 150 μm) through resonance frequency offsets, and its average sensitivity is 7.28 kHz/ μm , while its average sensitivity is 3.09 kHz/ μm [15]. With a sensitivity of 40.41, Q-factor of 950, and figure of merit of 52,002.9, as well as linear frequency shifts from 2.17 to 1 GHz across samples for food safety applications, a cylindrical-shaped resonator-integrated transmission line sensor has been suggested for noninvasive quality estimation of mustard oil [16]. A novel differential-mode planar microwave sensor has been designed for complex permittivity measurement of ethanol-water solutions. It combines a curved ring resonator with an annular microstrip transmission line. By utilizing a backpropagation neural network, the sensor achieves an average sensitivity of 1.184% and a maximum error of less than 3.5% [17]. A convolutional neural network and a miniature microstrip microwave sensor were used to non-contactly detect fasting blood sugar from 78 people's samples. The estimated FBS values for biomedical monitoring had an average relative error of 1.31% [18]. An innovative microwave sensor with four bands operating from 0.5 to 3.2 GHz and a sensitive area that can handle 1 mL samples has been developed. It can detect alcohol-water and herbicide mixtures with a maximum sensitivity of 1.12% and is thus well-suited for environmental monitoring [19]. Ebrahimi *et al.* [20] introduced a microwave

biosensor for glucose detection in aqueous solutions. It is label-free and reflective, yet limited by weak contrast between water and glucose permittivity.

This research distinguishes itself by introducing a highly sensitive, compact, and non-contact microwave-based sensor designed for precise measurement of volume percentages in water and crude oil mixtures. Unlike previous sensors that either lacked sensitivity, required complex calibration procedures, or relied on contact-based measurement setups, the proposed sensor operates efficiently within the 2–2.3 GHz frequency range and demonstrates a sensitivity of 4.12 MHz/ ϵ_r , surpassing many state-of-the-art alternatives. By incorporating multiple U-shaped resonators and a novel layout optimized through rigorous electromagnetic simulations, this sensor achieves low insertion loss, stable performance, and clear frequency response characteristics. Its non-contact measurement method- achieved by positioning samples in a dielectric container above the sensor surface- not only enhances reliability but also minimizes contamination risks, making it well-suited for real-world industrial applications. This work offers a robust, scalable, and efficient solution for real-time fluid composition analysis, with potential applications in petroleum and environmental monitoring.

To enhance the readability and comparability of the literature review presented in the Introduction, Table 1 provides a structured summary of ten recent studies on microwave-based sensors for liquid mixture characterization and quality assessment. This table highlights key aspects such as sensor design, primary applications, performance characteristics, and the incorporation of neural networks, facilitating direct comparison with the proposed multiple U-shaped resonator sensor and underscoring its contributions in sensitivity, non-contact operation, and compactness.

Table 1. Overview of recent microwave sensors for liquid analysis and quality detection

Ref.	Sensor Type	Application	Key Features/Performance	Neural Network Used
[2]	Microstrip with dual passbands	Non-contact volume fraction measurement of oil-water mixtures (independent of sample volume)	High accuracy; compact; non-contact; robust to sample volume variations	<i>Multilayer Perceptron (MLP)</i>
[3]	Microstrip antenna with quasi-circular resonator	Oil-water biphasic mixture volumetric content analysis	Average sensitivity 4.26 MHz/%; RMSE <0.93; R ² =0.99; multi-resonance	<i>Group Method of Data Handling (GMDH)</i>
[10]	Planar <i>split-ring resonator (SRR)</i> with defected ground gap-coupled transmission line	Real-time non-contact water-cut measurement in crude oil (bitumen/heavy oil)	Frequency shift: 69.75–70.5 MHz full range; small sample volume (~1.424 mL); non-invasive	None
[11]	<i>Substrate Integrated Waveguide (SIW)</i> resonator	Detection and quantification of water contamination in fuel oil (0–100%)	Sensitivities: 0.12 dB/% and 0.88 MHz/%; non-contact; operating range 1.50–1.55 GHz	<i>Multilayer Perceptron (MLP)</i>
[14]	Microstrip with dual passbands	Real-time milk spoilage detection	Amplitude difference 7.02 dB; training accuracy 95.5%; validation 90%; non-destructive	<i>Convolutional Neural Network (CNN)</i>
[15]	Microstrip line-coupled <i>split-ring resonator (SRR)</i> with microfluidic channel	Detection of contaminants (metal particles, air bubbles) in lubricating oil	Detection limits: 70 μ m metal, 150 μ m bubbles; sensitivity 7.28/3.09 kHz/ μ m; high SNR	None
[16]	<i>Cylindrical-shaped resonator-integrated transmission line (CRITL)</i>	Mustard oil quality estimation	Sensitivity 40.41; Q-factor 950; FoM 52 002.9; noninvasive	None
[17]	Differential curved ring resonator with annular microstrip transmission line	Permittivity determination of ethanol-water solutions	Average sensitivity 1.184%; error <3.5%; differential mode for noise immunity	<i>Backpropagation Neural Network (BP-NN)</i>
[18]	Miniaturized broadband microstrip	Non-contact detection of fasting blood sugar (FBS) in human blood samples	Mean relative error 1.31%; real clinical samples; broadband operation	<i>Convolutional Neural Network (CNN)</i>
[19]	Multi-band one-port interdigitated split-ring resonator	Detection of liquid mixtures (e.g., water-alcohol, water-herbicide)	Four resonances (0.5–3.2 GHz); max sensitivity ~1.12%; small sample volume (1 mL)	None

2. Design and simulation procedures

The extensive application of sensors in biological detection and environmental monitoring continues to grow. Despite the significant advancements in microstrip sensors for detecting biological and physical processes, there remains a need for further improvements. A primary limitation of these sensors stems from the complex interactions between electromagnetic fields and the dielectric properties of the materials surrounding the sensor. The frequency response characteristics of a sensor may be drastically affected by changes in the relative permittivity of materials close to its surface. The use of precise mathematical models and physical equations can provide valuable insights into the wide range of changes that occur. Alterations in the relative permittivity of the substances used to microstrip sensors may lead to significant changes in their electromagnetic characteristics, including frequency resonance and IL. These variations typically manifest as shifts in the localized electromagnetic field surrounding the microstrip structure. The relative permittivity of the substrate material is a key factor influencing the intrinsic properties of a microstrip sensor. As a result, the frequency response of the sensor may be impacted in various ways by the substrate. The electromagnetic fields around the sensor can be affected by changes in the material immediately adjacent to it. To what degree these effects manifest depends on electrical qualities of the surrounding material, the system's physical configuration, and parameters like relative permittivity, electrical conductivity, and permeability to magnetic fields. Maxwell's equations [21] provide a framework for a detailed examination of these influences.

$$\nabla \cdot D = \rho, \quad (1)$$

$$\nabla \cdot B = 0, \quad (2)$$

$$\nabla \times E = -\frac{\partial B}{\partial t}, \quad (3)$$

$$\nabla \times H = J + \frac{\partial D}{\partial t}. \quad (4)$$

The following is a definition of each of the equation's variables: The electric charge density is denoted by ρ , the electric current density is denoted by J , the electric field is represented by E , B stands for the electrical flux density, H for the magnetic field. and the electric charge density is represented by E . Material equations [21] often demonstrate the link between D and E fields and B and H fields:

$$D = \varepsilon E, \quad (5)$$

$$B = \mu H. \quad (6)$$

In this context, ε represents the media's permittivity and μ stands for the medium's magnetic permeability. When a *material under test* (MUT) is placed in close proximity above the microstrip sensor—without direct physical contact—the following relationships are modified through the influence of the effective permittivity (ε_{eff}):

$$D = \varepsilon_{eff} \varepsilon_0 E, \quad (7)$$

$$B = \mu_{eff} \mu_0 H. \quad (8)$$

In this context, ε_0 signifies the permittivity of free space, while ε_{eff} refers to the effective permittivity of the microstrip sensor. The effective permittivity ε_{eff} combines the effects of the sensor and substrate materials on the resonance frequency (f_r) [22]:

$$f_r = c/2\pi \sqrt{\varepsilon_{eff} \cdot \varepsilon_0 \cdot \mu_0 \cdot \left(\frac{h}{h_{eff}}\right) \cdot \left(\frac{w}{w_{eff}}\right)}. \quad (9)$$

In this context, c represents the speed of light in a vacuum, while h is the height of the substrate, and h_{eff} refers to the effective height, which considers the effects of both the substrate and the surrounding materials on the sensor's performance. Similarly, w indicates the width of the microstrip, and w_{eff} signifies the effective width, which incorporates the influence of dielectric materials. To calculate the effective permittivity (ϵ_{eff}), several approaches are employed, tailored to the specific design and structure of the microstrip. These approaches include convex mapping and experimental formulae for diverse setups.

In conclusion, the interplay between the relative permittivity of the sensor and substrate materials establishes a strong relationship between the resonance frequency and the effective permittivity of a microstrip sensor. There is a complex relationship between the microstrip structure and its electromagnetic and geometrical characteristics. Many empirical approaches consider the relationship between the material's permittivity ($\epsilon_{r.material}$) and the substrate's permittivity ($\epsilon_{r.sub}$) when estimating the effective permittivity (ϵ_{eff}) of a microstrip sensor. When designing microstrip systems, the parallel plate capacitor idea is a common starting point. Effective permittivity in microstrip structures may be expressed using the following commonly used empirical formula:

$$\epsilon_{eff} = \epsilon_{r.sub} + \frac{\epsilon_{r.material} - \epsilon_{r.sub}}{1 + \frac{h}{t} \left(\frac{\epsilon_{r.material} - 1}{\epsilon_{r.sub}} \right)} \quad (10)$$

In the first stage, two U-shaped resonators were placed next to each other at a distance of 0.25 mm. Figure 1a displays the layout of this structure. This structure, as shown, offers an unsuitable pass band within the frequency range of approximately 2.1 GHz. We added another U-shaped resonator to the structure (Fig. 1b) to improve the frequency response and reduce the sensor's insertion loss. Despite achieving a significant improvement in the sensor's insertion loss with the addition of this resonator, the sensor's bandwidth remained low. We added another U-shaped resonator to the circuit structure to improve the bandwidth, but the sensor's insertion loss in the passing band had not yet reached a suitable value (Fig. 1c). The final structure of the introduced sensor has five U-shaped resonators (Fig. 1d). This structure has a passband between frequencies of 2 to 2.3 GHz with a maximum insertion loss of 0.97 dB. Figure 2 shows the frequency response of the introduced sensor in four stages of design. The dimensions of the sensor under consideration are $36.41 \times 20 \text{ mm}^2$, and it is mounted on an RT/Duroid 4003 substrate, which has a relative permittivity (ϵ_r) of 3.55, a thickness of 0.787 mm, and a loss tangent of 0.0022. The simulation of the proposed sensor is carried out using the *Advanced Design System (ADS) Electromagnetic Simulator* (EM Simulator).

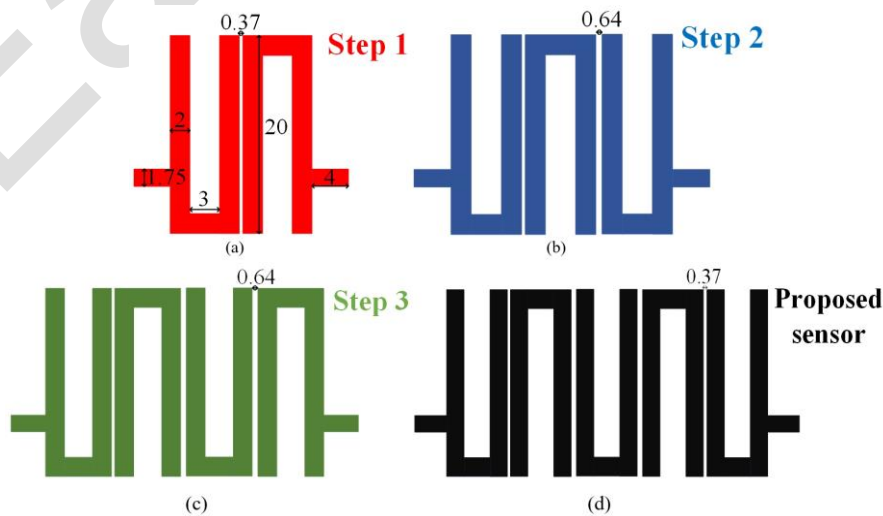


Fig. 1. Proposed sensor structures (description in text).

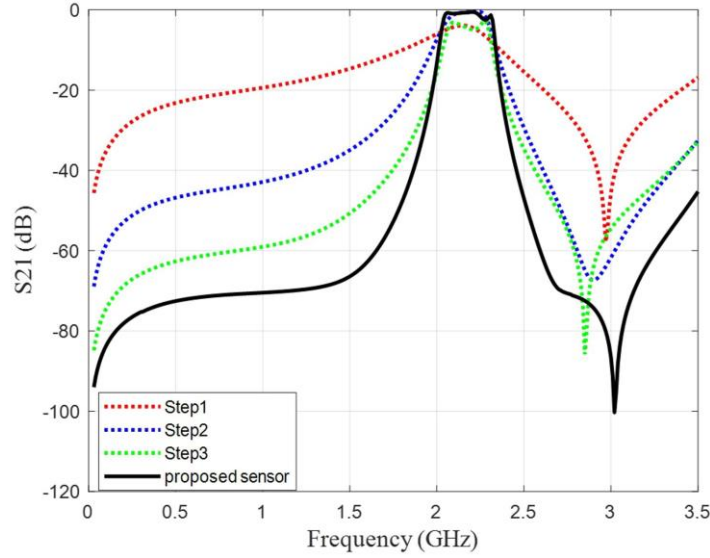


Fig. 2. Frequency response of the proposed sensor through its design stages: Step 1 (red), Step 2 (blue), Step 3 (green), and the final proposed sensor (black)

The equivalent inductance of a microstrip line can be calculated using various empirical formulas that take into account the dimensions and characteristics of the microstrip line. commonly used formula for calculating the inductance per unit length L' for a microstrip line are given by [22]:

$$L' = \frac{\mu}{4\pi} \ln \left(\frac{2h}{w} + 1.08 \right). \quad (11)$$

The formula takes the substrate material permeability μ in H/m, the substrate height h in m, and the width of the microstrip line w in m, where L' is the inductance per unit length (H/m). A microstrip line's total inductance L may be calculated by multiplying its inductance per unit length L' by the length of the line l :

$$L = L' \cdot l. \quad (12)$$

The interaction between two microstrip lines is primarily characterized by two main capacitive effects. Figure 3 illustrates the capacitors C_{gd} and C_{ga} , which represent the capacitive effects between the two microstrip lines. C_{gd} corresponds to the capacitive effect with the dielectric of the substrate, while C_{ga} represents the capacitive effect with air. The capacitance C_f represents the fringe capacitance, whereas C_p refers to the parallel plate capacitance between the strip and the ground plane [23].

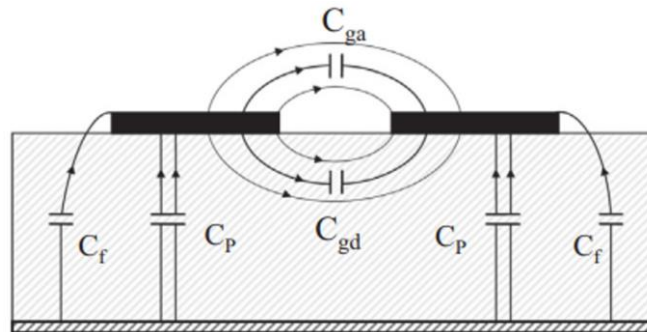


Fig. 3. Symmetric coupled microstrip lines.

The formulae for these capacitors are provided in reference [23]. The coupling capacitance C_g is composed of two capacitances: C_{ga} , which represents the capacitance for the field in the air, and C_{gd} , which represents the capacitance for the dielectric substrate [24]:

$$C_g = C_{gd} + C_{ga}. \quad (13)$$

The value of these capacitors could be determined using the following formulae [25]:

$$C_{gd} = \varepsilon_{r.sub} \cdot \varepsilon_0 \frac{\kappa(k')}{\kappa(k)}, \quad (14)$$

$$C_{ga} = \varepsilon_0 \frac{\kappa(k')}{\kappa(k)}, \quad (15)$$

where:

$$k^2 = (1 + 2\frac{w}{s}) / (1 + \frac{w}{s})^2, \quad (16)$$

$$k' = \sqrt{1 - k^2}. \quad (17)$$

The symbol ε_0 represents the permittivity of free space, whereas $\frac{\kappa(k')}{\kappa(k)}$ denotes the ratio of the elliptic functions. Precise and straightforward formulas for the ratio $\frac{\kappa(k')}{\kappa(k)}$ could be found in reference [25].

It is possible to compute the capacitance C_g precisely by using (13) to (17). Figures 4 show the LC equivalent circuit of the sensor and Fig. 5 show its frequency response. Table 2 presents the values of the inductor and capacitor in the LC equivalent circuit. Equations (13) to (17) could be used to compute the values of the C_3 and C_4 capacitors. These capacitors serve as the equivalent coupling capacitors between the microstrip lines. If a material is present on the sensor, it will alter the value of the capacitors, resulting in a modification of the sensor's frequency response. Figure 6 shows the corresponding circuit's frequency response when capacitors C_3 and C_4 are altered. From the above figure, it is evident that raising the capacitance value will result in a reduction in both the bandwidth and the center frequency of the passband.

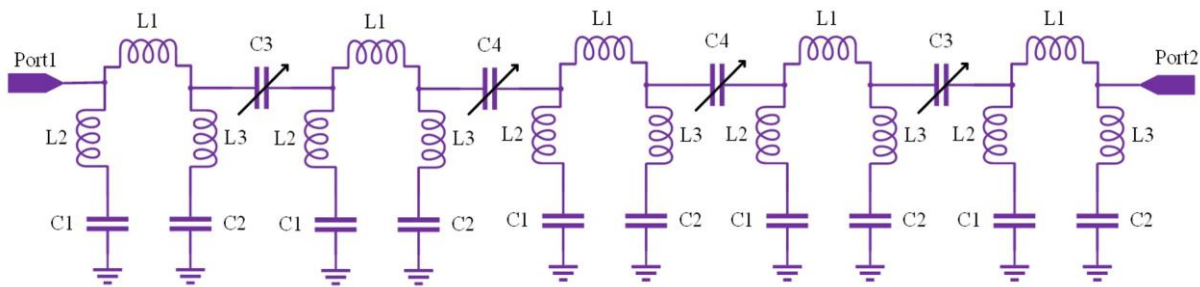


Fig. 4. LC equivalent circuit of proposed sensor.

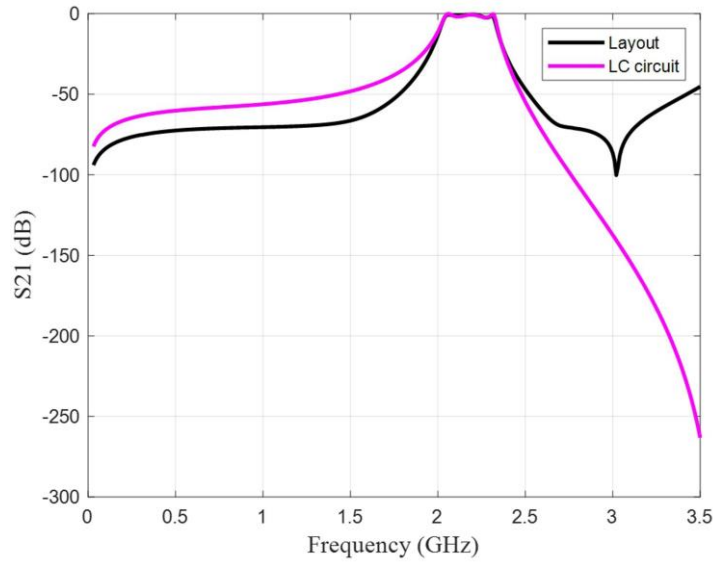


Fig. 5. Frequency response of layout and LC equivalent circuit.

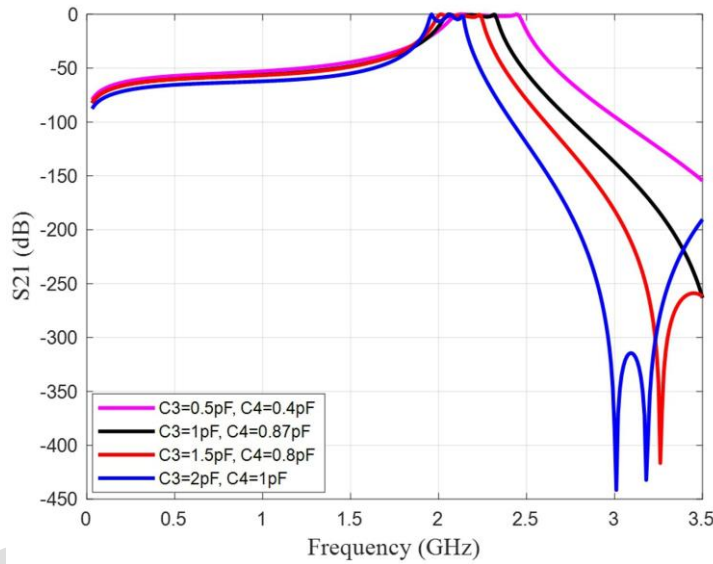


Fig. 6. The effect of C_3 and C_4 capacity changes on the frequency response.

Table 2. Capacitor and inductor values of LC equivalent circuit.

C1 (pF)	C2 (pF)	C3 (pF)	C4 (pF)	L1 (nH)	L2 (nH)	L3 (nH)
2	2	1	0.87	2.8	0.98	0.8

3. Results and discussion

The simulated sensor in the previous section was fabricated on a RT/Duroid 4003 (with $\epsilon_r = 3.55$ and a thickness 0.787 mm) substrate. Also, a box made of *polylactic acid* (PLA) material for placing oil and water solutions on the sensor with dimensions of $11 \times 22 \times 40 \text{ mm}^3$ was made using a 3D printer. The wall thickness of the box was 1 mm. The PLA box design incorporates clamps to ensure the box remains stationary on the sensor throughout all tests. Figure 7 shows the frequency response of the fabricated sensor compared to the simulation results. It should be noted that placing the PLA box on the sensor will cause changes in the frequency response, but due to the fact that these changes are constant in all tests, they can be

ignored. In this research, samples of water and crude oil solutions were prepared in a laboratory environment with a participation percentage of 0% to 100% water in a solution volume of 10 ml. The solution samples were introduced into a PLA container and positioned atop the fabricated microstrip sensor. A total of 11 samples were examined, and their respective frequency responses were captured within a frequency span of 30 MHz to 3.5 GHz. The experimental setup is illustrated in Fig. 8. For capturing the sensor's frequency response, a Nano VNA-F V3 vector network analyzer was utilized.

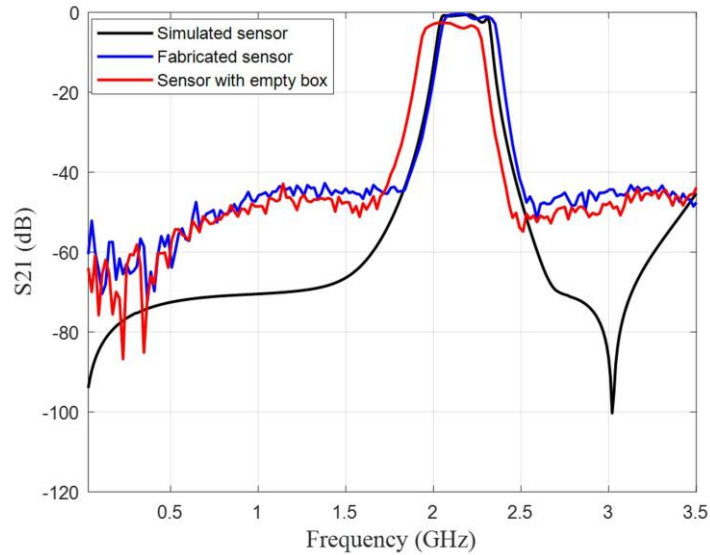


Fig. 7. Frequency response of fabricated, simulated, and empty-container sensors.

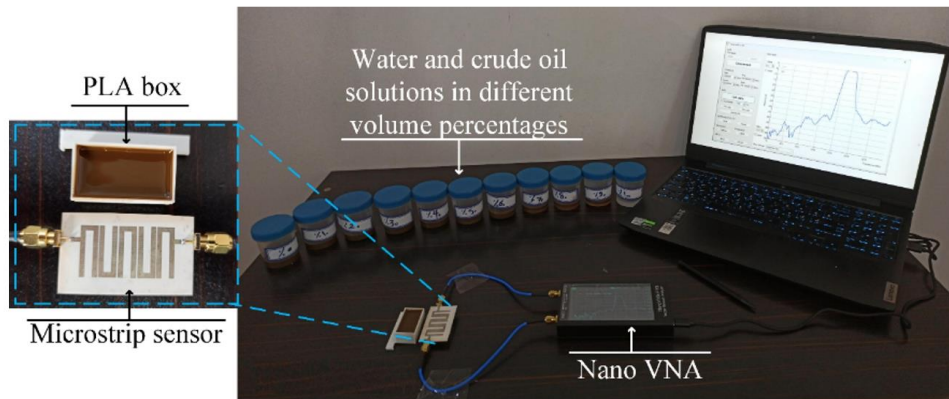


Fig. 8. Laboratory structure for measuring volume percentage of water- crude oil.

To achieve non-contact measurement, the water-crude oil mixture samples were contained within a 3D-printed PLA box (wall thickness 1 mm) that was securely positioned atop the sensor surface. This configuration ensures no direct physical contact between the liquid samples and the microstrip lines, thereby preventing contamination or damage to the sensor while allowing the electromagnetic fields to penetrate the thin PLA wall and interact with the sample's dielectric properties. The term 'non-contact' in this work specifically refers to the absence of direct liquid-sensor contact, distinguishing it from methods requiring immersion or direct deposition of the material under test.

To mitigate the potential influence of the underlying table surface on the fringing electric fields of the microstrip resonators, the sensor board was not placed directly on the table. Instead,

the coaxial cables connecting the sensor to the NanoVNA-F V3 were carefully bent to elevate the board several centimeters above the table surface, creating an air gap that prevented direct contact with the table material. This configuration, combined with rigid fixation of the setup, minimized variations due to the dielectric properties of the table or its coating. At the operating frequency of approximately 2.1 GHz, fringing fields extend beyond the substrate, and proximity to conductive or dielectric materials could indeed affect the overall capacitance and measurement accuracy. The air gap approach effectively reduced this influence in the controlled laboratory setting. Different types of crude oil have different relative permittivities at different temperatures and with different chemical compositions. However, numbers between 2 and 4 are typical. Due to the complex mixture of hydrocarbons and other elements, crude oil exhibits a wide range of electrical properties. Nonetheless, at around 25°C, pure water has a relative permittivity of roughly 78.5, frequently simplified to 80. The microstrip sensor's coupling capacitors will grow in proportion to the test material's permittivity, as shown in (13) – (17). A lower operating frequency will be the outcome of this increase in coupling capacitors.

Figure 9 shows the frequency response of the designed sensor under the test conditions of different solutions. As it is clear from this figure, by increasing the percentage of water in the oil-water solution, we will have a frequency shift of the pass band, an increase in the attenuation of the pass band, and also a decrease in the suppression level in the cut-off band of the sensor. In this case, it looks like the central frequency (F_c) of the pass band and the prominence of the frequency response could be two good ways to tell the difference between volume percentages. Figure 10 shows the extracted characteristics for two frequency responses: the 100% crude oil test and the 100% water test. As it is known, with the increase in water percentage, we will have a decrease in prominence and a decrease in F_c . The prominence of a peak, as defined in signal analysis, signifies the extent to which a peak stands out amidst the surrounding baseline of the signal. It provides a precise assessment of the peak's prominence within the data by representing the vertical distance between the peak and its lowest contour line. A higher prominence value indicates a peak that is more prominent and distinct from its surroundings, suggesting a clearer and more significant feature in the signal. Conversely, lower prominence values may suggest peaks that are less pronounced or potentially obscured by noise. The value of the characteristics extracted from the frequency response for each of the samples can be seen in Fig. 11.

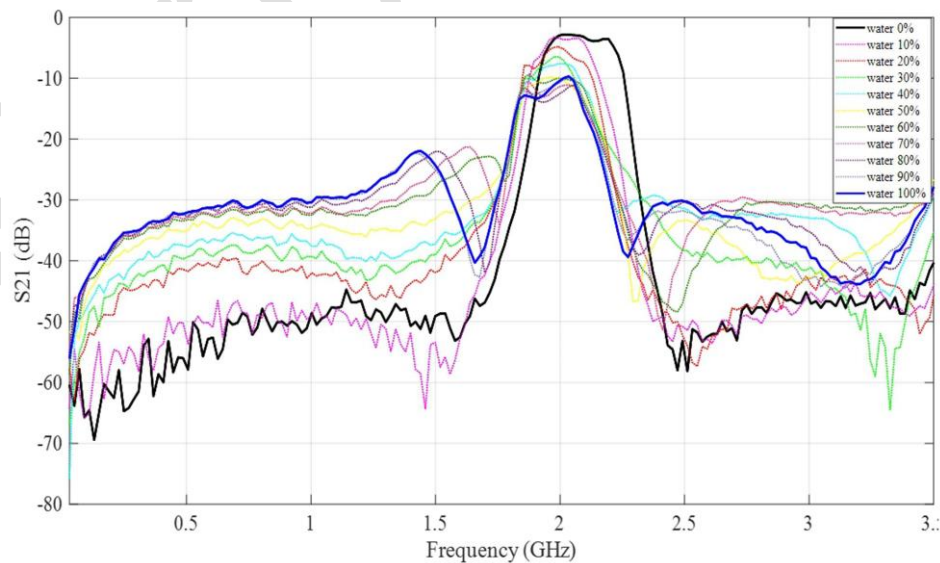


Fig. 9. Frequency responses recorded under test conditions of water-oil solutions with different volume percentages.

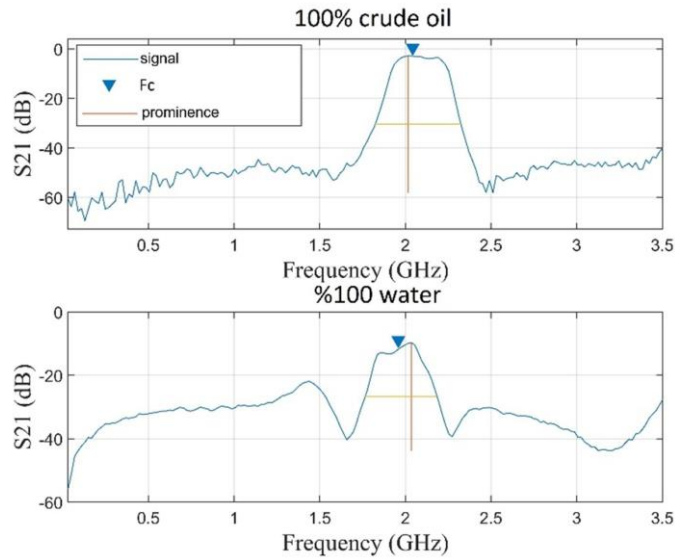


Fig. 10. Features extracted for the frequency response.

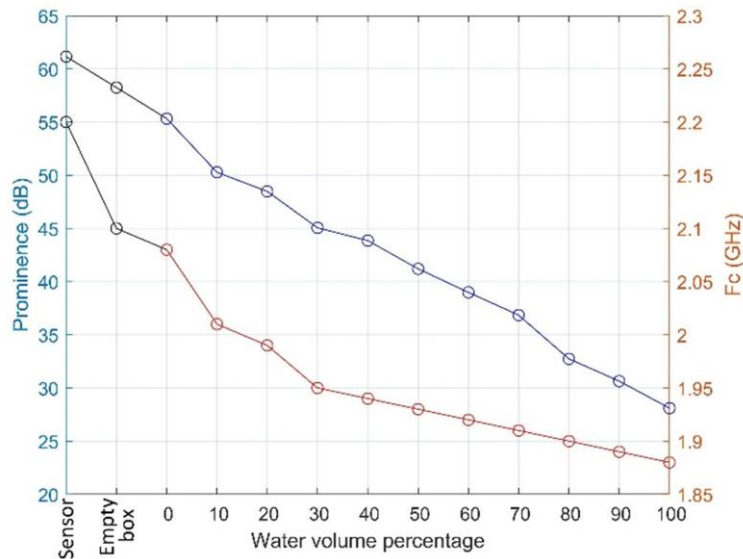


Fig. 11. Extracted features for all tested samples.

The water-crude oil mixture samples (10 ml volume) were prepared fresh in the laboratory immediately prior to each measurement by vigorous manual shaking for approximately 1 minute to form a temporary emulsion, ensuring initial homogeneity. Measurements were conducted promptly thereafter to limit the opportunity for phase separation. Microstrip resonators are particularly sensitive to the dielectric material in closest proximity to the sensor surface due to the concentration of fringing electric fields in that region. Consequently, if stratification occurs—with the denser water phase settling at the bottom near the sensor—the frequency shift and prominence reduction would disproportionately reflect higher water content, leading to overestimation. In a stable, uniformly distributed emulsion, however, the readings accurately represent the bulk volume percentage. No visual evidence of phase separation was noted in the PLA container post-measurement. Nevertheless, this represents a potential limitation for applications involving longer holding times or less stable mixtures. For enhanced reliability in practical scenarios, pre-measurement verification of emulsion homogeneity—such as through repeated agitation, visual inspection, or integration of a stirring mechanism—is recommended to prevent stratification-induced errors.

The sensitivity value of the sensor designed according to (18) was 4.12 MHz/ ϵ_r times, which is a significant value compared to previous research. Table 3 compares the developed sensor's performance with several sensors from previous studies in terms of dimensions, sensitivity, operational frequency, and resonator type.

$$\text{Sensitivity} = \frac{|F_{C_w} - F_{C_0}|}{\epsilon_w - \epsilon_0}. \quad (18)$$

When the pass band is filled with 100% water, the center frequencies are denoted as F_{C_w} , and when they are empty, they are denoted as F_{C_0} . Whereas ϵ_w represents the relative permittivity of water, ϵ_0 represents the relative permittivity of free space.

Table 3. Comparison of the features of the designed sensor with previous researches.

Ref.	Resonator architecture	Resonant frequency (GHz)	Sensors sizes (mm)	Sensitivity (MHz)/ ϵ_r
[26]	SRR	1.9	7×9.35	1.53
[27]	SRRs	0.87	86×62	0.79
[28]	CSSRRs	5.35 and 7.99	30 × 25	0.04
[29]	OCSRRs	0.9	46 × 46	1.8
[30]	CSRR	2.85 and 2.96	28 × 20	3.0
[this work]	U-shape resonator	2 to 2.3	36.41×20	4.12

All measurements were performed in a standard university laboratory environment without the use of a dedicated shielded room or anechoic chamber. Short, high-quality shielded coaxial cables were employed to connect the sensor to the NanoVNA-F V3, and tests were conducted during periods of low ambient activity to minimize potential interference. Throughout the experiments, no noticeable distortions in the S21 transmission parameters attributable to external electromagnetic signals were observed, indicating sufficient stability for controlled laboratory conditions. However, the operating frequency range (2–2.3 GHz) overlaps with common communication bands (e.g., Wi-Fi and Bluetooth around 2.4 GHz), and the VNA's high sensitivity as a receiver could make it susceptible to external radiation in noisier environments. Such interference might distort the amplitude of S21 or shift the apparent resonant frequency. For real-world applications in industrial or field settings with higher electromagnetic activity, the use of electromagnetic shielding (e.g., a metallic enclosure around the sensor and sample) or additional RF filtering is recommended to enhance measurement robustness and accuracy.

The utilization of a 3D-printed PLA container (wall thickness 1 mm) facilitates rapid prototyping and ensures non-contact measurement by preventing direct liquid exposure to the sensor surface. However, PLA is not an ideal dielectric material for precision microwave applications, as its relative permittivity typically ranges from 2.5 to 3.2 and it exhibits variability due to moisture absorption from the ambient environment as well as microporosity introduced during the additive manufacturing process. These factors can potentially alter the effective loss tangent and introduce minor inconsistencies in the electromagnetic field interaction. In the present experiments, all measurements were conducted in a controlled laboratory setting over short durations with consistent humidity levels. Prior to introducing each new sample, the frequency response of the sensor with the empty PLA container was measured and compared to the initial baseline reference (as shown in Fig. 7) to verify that it remained unchanged, thereby confirming the absence of distortions arising from container-related effects such as moisture uptake. No significant distortions attributable to container variability were observed across the tested samples. Nonetheless, to mitigate these potential effects and enhance

long-term stability and measurement accuracy, future implementations should employ low-loss, moisture-resistant materials for the sample holder, such as PTFE (Teflon, $\epsilon_r \approx 2.1$ with very low loss tangent), quartz glass, or *high-density polyethylene* (HDPE).

The PLA container incorporated integrated clamps to ensure secure, repeatable, and tight placement on the sensor surface, minimizing potential air gaps or positional variations. To address possible inconsistencies - such as unevenness in the bottom thickness of the 3D-printed container or imperfect fit - a calibration procedure was implemented before each new measurement series or container repositioning. This involved recording the frequency response with the empty PLA container and comparing it to the initial baseline reference (as illustrated in Fig. 7). This step allowed verification of positioning consistency and detection of any parasitic air gaps that could distort the electric field lines and introduce errors in frequency shift. Across all tests, the empty-container responses exhibited high reproducibility, with center frequency deviations of less than 0.5 MHz and negligible changes in insertion loss, confirming effective mitigation of such effects in the controlled laboratory setup. No significant measurement errors attributable to these factors were observed in the reported results. However, in practical applications with varying environmental conditions or less precise container fabrication, these issues could contribute to variability. Future improvements should focus on using precision-fabricated containers (*e.g.*, machined PTFE or glass with certified flatness and uniform thickness) and incorporating mechanical or optical alignment mechanisms to guarantee sub-millimeter positioning accuracy and eliminate parasitic air gaps.

The results of this study demonstrate the successful design, fabrication, and characterization of a microstrip sensor tailored for non-contact measurement of volume percentages in water and crude oil solutions. Operating within the frequency range of 2 to 2.3 GHz, the sensor exhibited high sensitivity, as evidenced by significant shifts in frequency responses upon analyzing different volume percentages of the solution samples. Particularly noteworthy was the sensor's ability to effectively distinguish between various volume percentages, highlighting the prominence of frequency response as a crucial parameter in fluid analysis. The exceptional sensitivity of 4.12 MHz/ ϵ_r underscores the sensor's potential for precise and reliable measurements. Moreover, the non-contact nature of the measurement setup not only enhances convenience but also minimizes potential interference, thereby enhancing the sensor's robustness for real-world applications. These findings not only validate the efficacy of the proposed sensor design but also contribute to the advancement of sensor technologies in fluid analysis across diverse industrial sectors, including petroleum, chemical, and environmental monitoring.

The experiments reported in this study were performed at a controlled room temperature of approximately 25°C, at which the relative permittivity of pure water is approximately 78.5 and that of crude oil typically ranges between 2 and 4, depending on its specific composition. It is acknowledged that temperature variations can substantially influence the dielectric properties of water-crude oil mixtures, as rising temperature generally reduces the permittivity of water due to decreased molecular polarization and may also alter the effective permittivity of crude oil through changes in viscosity and molecular structure. Although the sensor exhibited consistent and reliable performance under the tested constant-temperature conditions, the effects of temperature fluctuations on frequency shift, insertion loss, and overall measurement accuracy were not systematically investigated in this work. This represents a potential limitation for applications in environments with significant thermal variations. Future investigations should incorporate temperature-controlled testing across a wider range (*e.g.*, 10–60°C) to quantify these effects and develop calibration or compensation strategies to further enhance the sensor's robustness in real-world industrial settings.

Looking ahead, further research avenues can be explored to enhance the capabilities and applicability of microstrip sensors in fluid analysis. Firstly, investigations into optimizing the

sensor's design parameters such as substrate material, geometry, and dimensions could potentially improve its sensitivity and performance. Additionally, exploring alternative frequency ranges or multi-frequency approaches may offer insights into expanding the sensor's detection range and versatility. Moreover, integrating advanced signal processing techniques, such as machine learning algorithms, could enable more sophisticated analysis and interpretation of sensor data, thereby enhancing accuracy and reliability. It would be helpful to satisfy varied industrial demands by expanding the spectrum of applicability to include a larger variety of fluid mixtures and conditions in the environment. Overall, future research endeavors should focus on advancing sensor design, refining measurement techniques, and exploring innovative applications to meet the evolving demands of fluid analysis in various industrial sectors.

4. Conclusion

This study introduces an innovative microwave-based sensor for non-contact measurement of volume percentages in water and crude oil mixtures. Extensive testing on an RT/Duroid 4003 substrate, along with precise modelling in ADS software, demonstrated the sensor's remarkable sensitivity within the 2 to 2.3 GHz frequency range. Experimental validation revealed significant shifts in frequency responses, highlighting the sensor's capability to accurately distinguish between different volume percentages with high precision. The non-contact measurement approach not only enhances convenience but also improves the sensor's robustness by minimizing potential interference. With a sensitivity of $4.12 \text{ (MHz)}/\epsilon_r$, this sensor shows strong potential for precise and reliable measurements in industries such as petroleum, chemicals, and environmental monitoring.

Future research should focus on optimizing the sensor's design parameters, exploring alternative frequency ranges, integrating advanced signal processing techniques, and expanding its application to meet the evolving needs of fluid analysis in various industrial sectors. Ultimately, this microwave-based sensor offers a promising opportunity to improve the efficiency and reliability of industrial fluid analysis by enabling accurate, non-invasive volume percentage measurements in water and crude oil mixtures.

Acknowledgments

This work was supported by the Deanship of Research and Graduate Studies at King Khalid University through the Large Research Project, grant number RGP2/225/45.

References

- [1] Han, X., Zhou, Y., Peng, P., Fu, C., Qiao, L., Zhang, Y., Liu, K., & Zhang, S. (2023). Microfluidic microwave sensor loaded with annular microstrip patch for lubricating oil quality inspection. *IEEE Sensors Journal*, 23(23), 28891–28898. <https://doi.org/10.1109/jsen.2023.3325733>
- [2] Sattari, M. A., & Hayati, M. (2024). Accurate and non-contact measurement of volume percentages of oil-water fluids using microstrip sensors independent of the volume of sample using artificial neural network. *Flow Measurement and Instrumentation*, 97, 102621. <https://doi.org/10.1016/j.flowmeasinst.2024.102621>
- [3] Sattari, M. A., & Hayati, M. (2024b). A novel approach to oil-water mixture analysis: Microstrip antenna-based sensor combined with GMDH neural network. *Flow Measurement and Instrumentation*, 101, 102751. <https://doi.org/10.1016/j.flowmeasinst.2024.102751>
- [4] Xue, Q., Tang, X., Li, Y., Liu, H., & Duan, X. (2019). Contactless and simultaneous measurement of water and acid contaminations in oil using a flexible microstrip sensor. *ACS Sensors*, 5(1), 171–179. <https://doi.org/10.1021/acssensors.9b01965>

- [5] Abdulsattar, R. K., Alibakhshikenari, M., Virdee, B. S., Sharma, R., Elwi, T. A., Kouhalvandi, L., Hassain, Z. a. A., Ali, S. M., Tokan, N. T., Livreri, P., Falcone, F., & Limiti, E. (2023). Optical-microwave sensor for real-time measurement of water contamination in oil derivatives. *AEU - International Journal of Electronics and Communications*, 170, 154798. <https://doi.org/10.1016/j.aeue.2023.154798>
- [6] Palandoken, M., & Gocen, C. (2025). Microwave sensor designs for liquid material dielectric characterization: Technological advances and applications. *Sensors and Actuators a Physical*, 387, 116381. <https://doi.org/10.1016/j.sna.2025.116381>
- [7] Jin, N., Liu, D., Bai, L., & Ren, Y. (2021). Measurement of water holdup in oil-in-water emulsions in wellbores using microwave resonance sensor. *Applied Geophysics*, 18(2), 185–197. <https://doi.org/10.1007/s11770-021-0893-3>
- [8] Wang, D., Jin, N., Ma, J., & Ren, Y. (2021). Measurement of water holdup in Oil–Gas–Water slug flow using microstrip antenna. *IEEE Transactions on Instrumentation and Measurement*, 70, 1–10. <https://doi.org/10.1109/tim.2021.3096574>
- [9] Zhu, L., Li, W., Han, X., & Peng, Y. (2020). Microfluidic flexible substrate integrated microstrip antenna sensor for sensing of moisture content in lubricating oil. *International Journal of Antennas and Propagation*, 2020, 1–9. <https://doi.org/10.1155/2020/9675847>
- [10] Kamal, B., Vestrum, S., BinDahbag, M. S., Abbasi, Z., & Hassanzadeh, H. (2024). Microwave-enabled chipless sensor for real-time non-contact water-cut measurements. *Measurement*, 228, 114314. <https://doi.org/10.1016/j.measurement.2024.114314>
- [11] Kongkeaw, P., Srisai, S., & Harnsoongnoen, S. (2025). Detection and quantification of water contamination in fuel oil using substrate integrated waveguide resonator-based microwave sensors coupled with multilayer perceptron neural networks. *Sensors and Actuators a Physical*, 384, 116280. <https://doi.org/10.1016/j.sna.2025.116280>
- [12] Ebrahimi, A., Scott, J., & Ghorbani, K. (2018). Differential sensors using microstrip lines loaded with two Split-Ring resonators. *IEEE Sensors Journal*, 18(14), 5786–5793. <https://doi.org/10.1109/jsen.2018.2840691>
- [13] Abdolrazzaghi, M., & Daneshmand, M. (2020). Exploiting sensitivity enhancement in micro-wave planar sensors using intermodulation products with phase noise analysis. *IEEE Transactions on Circuits and Systems I Regular Papers*, 67(12), 4382–4395. <https://doi.org/10.1109/tcsi.2020.3003010>
- [14] Khoshchehre, A., Sattari, M. A., Shah, U. H., & Roshani, G. H. (2025). Design and implementation of a microwave microstrip sensor with convolutional neural network for real-time milk spoilage detection. *Sensors International*, 7, 100353. <https://doi.org/10.1016/j.sintl.2025.100353>
- [15] Lv, B., Yang, X., Nie, B., Zhang, H., Zhang, Y., Qi, G., Li, S., Qiu, J., & Wei, R. (2024). A microwave sensor with Split-Ring resonator structure for the detection of lubricating oil contaminants. *IEEE Sensors Journal*, 24(10), 16845–16853. <https://doi.org/10.1109/jsen.2024.3386359>
- [16] Uddin, M. K., Alam, T., Islam, M. T., Kirawanich, P., & Baharuddin, M. H. (2025). Cylindrical-Shaped Resonator-Integrated transmission line based sensor for mustard oil quality estimation. *IEEE Sensors Journal*, 25(22), 41209–41218. <https://doi.org/10.1109/jsen.2025.3611271>
- [17] Han, X., Liu, K., Peng, P., & Zhang, S. (2025). Novel High-Sensitivity Differential Microwave Sensor for Permittivity Determination of Ethanol–Water Solutions. *IEEE Transactions on Instrumentation and Measurement*, 74, 1–11. <https://doi.org/10.1109/tim.2025.3552440>
- [18] Sattari, M. A., & Hayati, M. (2025). Detection of fasting blood sugar using a microwave sensor and convolutional neural network. *Scientific Reports*, 15(1), 22937. <https://doi.org/10.1038/s41598-025-06502-y>
- [19] Méndez-Jerónimo, G., Díaz-Arango, G. U., Álvarez-Botero, G. A., Lobato-Morales, H., & Molina-Reyes, J. (2025). Detection of liquid mixtures by using a novel microwave sensor based on a multi-band one-port interdigitated split ring resonator structure. *Journal of Microwave Power and Electromagnetic Energy*, 59(4), 303–320. <https://doi.org/10.1080/08327823.2025.2576656>
- [20] Ebrahimi, A., Scott, J., & Ghorbani, K. (2019). Microwave reflective biosensor for glucose level detection in aqueous solutions. *Sensors and Actuators a Physical*, 301, 111662. <https://doi.org/10.1016/j.sna.2019.111662>
- [21] Di Trocchio, L., Carucci, C., Sindhu, K. R., Morel, C., Lachaud, J. L., Bichon, S., Gounel, S., Mano, N., Boiziau, C., Dejous, C., Kuhn, A., & Hemour, S. (2020). Wireless in vivo biofuel cell monitoring. *IEEE*

- Journal of Electromagnetics RF and Microwaves in Medicine and Biology*, 5(1), 25–34. <https://doi.org/10.1109/jerm.2020.2998325>
- [22] Pozar, D. M. (2011). *Microwave engineering* (Fourth Edition). John Wiley & Sons, Inc.
- [23] Hong, J., & Lancaster, M. J. (2001). *Microstrip filters for RF/Microwave applications*. John Wiley & Sons, Inc. <https://doi.org/10.1002/0471221619>
- [24] Hayati, M., & Zarghami, S. (2019). Analysis of asymmetric coupling lines and design of a Wilkinson power divider based on harmonic suppression network. *AEU - International Journal of Electronics and Communications*, 115, 153047. <https://doi.org/10.1016/j.aecu.2019.153047>
- [25] Bedair, S. (1984). Characteristics of some asymmetrical coupled transmission lines (Short Paper). *IEEE Transactions on Microwave Theory and Techniques*, 32(1), 108–110. <https://doi.org/10.1109/tmtt.1984.1132620>
- [26] Withayachumnankul, W., Jaruwongrungee, K., Tuantranont, A., Fumeaux, C., & Abbott, D. (2012). Metamaterial-based microfluidic sensor for dielectric characterization. *Sensors and Actuators a Physical*, 189, 233–237. <https://doi.org/10.1016/j.sna.2012.10.027>
- [27] Velez, P., Su, L., Grenier, K., Mata-Contreras, J., Dubuc, D., & Martin, F. (2017). Microwave Microfluidic Sensor Based on a Microstrip Splitter/Combiner Configuration and Split Ring Resonators (SRRs) for Dielectric Characterization of Liquids. *IEEE Sensors Journal*, 17(20), 6589–6598. <https://doi.org/10.1109/jsen.2017.2747764>
- [28] Armghan, A., Alanazi, T. M., Altaf, A., & Haq, T. (2021). Characterization of dielectric substrates using dual band microwave sensor. *IEEE Access*, 9, 62779–62787. <https://doi.org/10.1109/access.2021.3075246>
- [29] Velez, P., Grenier, K., Mata-Contreras, J., Dubuc, D., & Martin, F. (2018). Highly-Sensitive microwave sensors based on open complementary split ring resonators (OCSRRs) for dielectric characterization and solute concentration measurement in liquids. *IEEE Access*, 6, 48324–48338. <https://doi.org/10.1109/access.2018.2867077>
- [30] Wang, C., Liu, X., Huang, Z., Yu, S., Yang, X., & Shang, X. (2022). A Sensor for Characterisation of Liquid Materials with High Permittivity and High Dielectric Loss. *Sensors*, 22(5), 1764. <https://doi.org/10.3390/s22051764>



Abdulilah Mohammad Mayet is currently an Associate Professor at King Khalid University, where he teaches courses in Nanofabrication and FPGA for Artificial Intelligence. He also serves as the CEO of Qimmam Abha Company, a subsidiary of the King Khalid University endowment. He received his master's and Ph.D. in Electrical Engineering with a focus on Microelectronics from King Abdullah

University of Science and Technology, where he collaborated closely with a co-advisor from Cornell University. His research experience includes partnerships with the Colleges of Engineering and Health Sciences at the University of California, Irvine. He also held the position of Visiting Professor at UC Irvine, during which he was awarded a prestigious Fulbright Fellowship for the 2023 and 2024 years. Additionally, he has been selected as a judge for the International Science and Engineering Fair in both 2024 and 2025. He has worked in leading technology hubs such as Silicon Valley, California, and Aix-en-Provence, France. His professional career includes founding and developing semiconductor fabrication and design facilities for microelectronics and MEMS-based sensors in organizations such as ETEC, ATMEL-ES2, and SEMC. His contributions to innovation have been recognized at esteemed institutions such as MIT, Cornell, IE Business School, and Esade.



Salman Arafath Mohammed is an Assistant Professor in the Department of Electrical Engineering (Computer Engineering Section) at the College of Engineering, King Khalid University, Saudi Arabia. He holds a B.Tech. in Computer Science and Information Technology, and an M.Tech. in Computer Science and Engineering, and a Ph.D. in Computer Science and Engineering. He previously worked

with IBM as a Senior Technical Engineer, contributing to AT&T and SBC projects, where he gained extensive experience in enterprise systems, network management, and large-scale telecommunications infrastructure. Before joining King Khalid University, he served as a faculty member at Vasavi College of Engineering and Keshav Memorial Institute of Technology (KMIT), where he was actively involved in teaching, research, and mentoring students to develop industry-ready technical and professional skills. His research interests include wireless sensor network security, routing protocols, ambient intelligence, Internet of Things (IoT), cyber security, machine learning, neural networks, and the application of intelligent computing technologies in healthcare systems.



Robert Hanus received his Ph.D. from Lviv Polytechnic National University (Ukraine) and his D.Sc. from Rzeszów University of Technology (Poland) in 1997 and 2016, respectively. He is currently employed as a full professor and the head of the Department of Metrology and Diagnostic Systems at the Faculty of Electrical and Computer Engineering at Rzeszów University of Technology. His scientific interests

include signal processing of random signals, measurement systems, and two-phase flow measurement, especially using radioisotope methods. He is the author or co-author of over 200 papers.



Shamimul Qamar is working as a University Professor (presently at King Khalid University Abha, Saudi Arabia) and an eminent scholar in the field of Computer Science & Eng. He had done his B.Tech from MMMUT Gorakhpur, M.Tech from AMU, Aligarh, and earned his Ph.D degree from IIT Roorkee with highly honorable grade. Prof. Qamar has a wide teaching experience in various engineering

colleges. He has research interests in Computer Networks & Security, Artificial Intelligence, and Internet applications. He was selected as a full Professor MIET/UPTU Lucknow in July 2007. He worked as a Director & Professor at KIT Kanpur. He has published several research papers in reputed national and international journals and conferences. He is a reviewer of IEEE, Springer, Elsevier, MDPI, *etc.* He authored text books and chapters in the field of Electronics & Computer Engineering. He is a lifetime member of the International Association of Engineers and a lifetime member of the Indian Society of Technical Education. His technical depth and interest resulted in setting up a research lab according to latest technical innovations. Along with this, he has actively participated in various technical courses, workshops, seminar *etc.* at IITS.



Hassen Loukil is an Assistant Professor in the Department of Electrical Engineering at King Khalid University. He received his Ph.D. and M.Sc. degrees in Electronics and his B.Sc. degree in Electrical Engineering from National Engineering School of Sfax. His primary research interests include image and video processing, hardware implementation using FPGA

technology, Embedded Systems and Algorithm-Architecture Matching. He has authored several peer-reviewed publications in reputed international journals and conference proceedings.



Neeraj Kumar Shukla is an Associate Professor in the Department of Electrical Engineering at King Khalid University. He received his Ph.D. in Digital VLSI Design and Memory Design from Uttarakhand Technical University, and his M.Tech and B.Tech degrees in Electronics Engineering from the University of Allahabad. He has over 25 years of academic and industry experience in electronics and

semiconductor engineering. His primary research interests include digital VLSI design, low-power SRAM design and characterization, memory architecture optimization, RTL-based ASIC/FPGA design methodologies, and nanoscale CMOS technologies. He has authored several peer-reviewed publications in reputed international journals and conference proceedings. Dr. Shukla has supervised five Ph.D. scholars and over thirty master's theses, in addition to guiding numerous undergraduate research projects. He has contributed to funded research initiatives and actively participates in industry-oriented VLSI skill development programs aimed at strengthening academia-industry collaboration in the semiconductor domain.

Early A